Vol.1 (2) (2020)

Measurement, control and automation

Website: https://mca-journal.org

ISSN 1859-0551

Modeling and Control of Wind-Solar-Battery Energy System – Energetic Macroscopic Representation Approach

Hoai-Linh T. Nguyen[1], Thanh Vo-Duy[1*], Bảo-Huy Nguyễn[1,2], Minh C. Ta[1,2] and João Pedro F. Trovão[2,3,4]

[1]*CTI Lab for EVs, School of Electrical Engineering, Hanoi University of Science and Technology, Hanoi, Vietnam*
[2]*e-TESC Lab., Université de Sherbrooke, Sherbrooke, QC, J1K 2R1, Canada*
[3]*INESC Coimbra, DEEC, University of Coimbra, Polo II, 3030-290 Coimbra, Portugal*
[4]*Polytechnic Institute of Coimbra, IPC-ISEC, DEE, 3030–199, Coimbra, Portugal*
[*]*E-mail: Linh.NTH202541M@sis.hust.edu.vn, thanh.voduy@hust.edu.vn, {Bao.Huy.Nguyen, Cao.Minh.Ta, Joao.Trovao}@USherbrooke.ca*

Abstract

Alternative energy sources, especially solar and wind energy, play an important role in the near future. However, building systems to make full use of them in areas without grids is still a problem that requires many studies. A commonly used system configuration is solar-wind energy system combined with a battery storage system. Recognizing that the modeling and control design of this mixed system by conventional methods is complex, this paper employs an effective approach using Energetic Macroscopic Representation (EMR) to represent a renewable energy conversion system model including solar and wind power combined with a battery system. Thanks to this formalism tool, control development for this complex system is straightforward. Besides, the maximum power point tracking strategy is applied to maximize the energy received from environment. The studied grid-isolated wind-solar-battery power system is simulated in MATLAB/Simulink under various real-world conditions to validate the reliability of the proposed method. The results confirm that this system always satisfies the loads power demand with the stably DC bus voltage.

Keywords: *Renewable energy, Battery, Energetic Macroscopic Representation, Maximum power point tracking*

Abbreviations

EMR	Energetic Macroscopic Representation
MPPT	Maximum Power Point Tracking
IPM	Interior Permanent Magnet
WECS	Wind Energy Conversion System
SECS	Solar Energy Conversion System
WSB	Wind-Solar-Battery

Tóm tắt

Năng lượng tái tạo sẽ đóng vai trò quan trọng trong một tương lai không xa. Tuy nhiên, việc xây dựng hệ thống nhằm tận dụng tối đa những nguồn năng lượng này ở những nơi không có điện lưới hiện vẫn đang là một vấn đề cần nhiều nghiên cứu. Một cấu hình hệ thống thường thấy đó là sự kết hợp giữa hệ thống năng lượng gió, năng lượng mặt trời và hệ thống lưu trữ bằng pin. Nhận thấy rằng việc mô hình hóa và điều khiển cho hệ thống kết hợp này bằng những phương pháp truyền thống khá phức tạp, bài báo này sẽ đề xuất một hướng tiếp cận hiệu quả sử dụng phương pháp biểu diễn vĩ mô năng lượng (EMR). Với công cụ đồ họa trực quan này, việc thiết kế cấu trúc điều khiển cho hệ thống phức tạp này sẽ trở nên rõ ràng và dễ thực hiện. Bên cạnh đó, thuật toán tìm điểm công suất cực đại cũng được áp dụng nhằm tối đa hóa năng lượng thu được từ tự nhiên. Việc sử dụng hệ thống năng lượng trên cung cấp cho tải độc lập không nối lưới được mô phỏng bằng phần mềm Matlab/Simulink trong những điều kiện thực tế nhằm kiểm chứng độ tin cậy của phương pháp mà bài báo này đưa ra. Kết quả mô phỏng cho thấy hệ thống luôn đáp ứng được yêu cầu công suất từ phía tải với điện áp ổn định trong mọi trường hợp.

1. Introduction

Currently, most of consumed energy come from thermal power, hydroelectric power or nuclear power plants. However, these sources may have adverse environmental consequences such as greenhouse gases emission, risks of radioactive leakage and ecosystem destruction. In addition, fossil fuel sources such as: coal, oil and natural gas are gradually depleted. As a reasonable substitution, renewable energy is becoming more common in power generation systems in order to replace the exhaustible energy sources. In particular, wind and solar energy are the promising choices.

Solar energy, which is considered the endless one, can be exploited in all regions of the world every day. It is able to used for various purposes such as: to produce electricity in areas without grids, to dry agricultural products or to supply space station. Another benefit of the solar energy systems is the relatively low maintenance cost. Besides, the material science is steadily evolving that leads to considerable potential

Submitted: 14 March 2021; Accepted: 3 May 2021.

to increase the performance of solar panel several times than before. Similar to solar energy, wind is also a source of energy which has great expectation to meet human needs. Moreover, the operating cost of the wind power system is lower than that in the past thanks to technological advances. It can be seen that these strong points of two energy resources will open up prospects for significant growth in the new era of green energy usage [1].

In spite of these aforementioned positive aspects, several typical drawbacks have to be solved. Firstly, solar and wind energy sources are unstable because of the dependence on the environment or weather. There are many studies giving solutions to overcome this problem, such as: static synchronous compensator and unified power flow controller are commonly used to diminish voltage fluctuation, harmonic distortion and frequency deflection of wind and photo-voltaic (PV) power plants [2, 3]. Secondly, it is still expensive and inconvenient to store energy for using when the solar and wind energy system are idle because of current technology problems, which can be seen in an overview of available energy storage technologies and their implementation is given in [4].

This paper focuses on modeling and control of a combination of renewable energy system to supply isolated loads. It can be seen in many research works available in literature that a suitable solution chosen to cope with the mentioned weaknesses of these natural energy sources is the sustainable energy systems. They combine with a battery system to maintain the stability of power supplies as well as to store energy when needed. The modeling and control design of the system are usually analyzed by conventional methods like frequency domain methods [5, 6] or time-domain state space representation [7, 8]. Nevertheless, they all have drawbacks that the modeling of the system is complex, the controls are difficult to design and the actual implementation may not be favorable. Accordingly, this paper proposes an different approach, which is using Energetic Macroscopic Representation (EMR) [9] based on action and reaction principle to represent the Wind-Solar-Battery (WSB) energy system model as interconnected subsystems obeying the integral causality. This formalism tool can handle the representation of complex energy system with only four main pictograms. Thanks to the ability of highlighting the system power flow, it is currently used for many studies of energy and electrical drive systems such as electric vehicles [10–12] and renewable energy systems [13–15]. After EMR of the studied system is built, the control schemes based on inversion principle can be deduced simply owing to the decomposed structure. Along with this system organization, maximum power point tracking (MPPT) control strategies are also applied in this paper due to their effectiveness and reliability [16–19].

The paper is organized as follows. Section 2 describes the system modeling. Section 3 presents the control design of the system and provides the energy management strategies. The simulation results are presented in Section 4. Finally, conclusions are conducted in Section 5.

2. System Modeling

2.1. EMR principle

The entire energy conversion system configuration is depicted in Fig. 1. Based on this configuration, the energetic system is

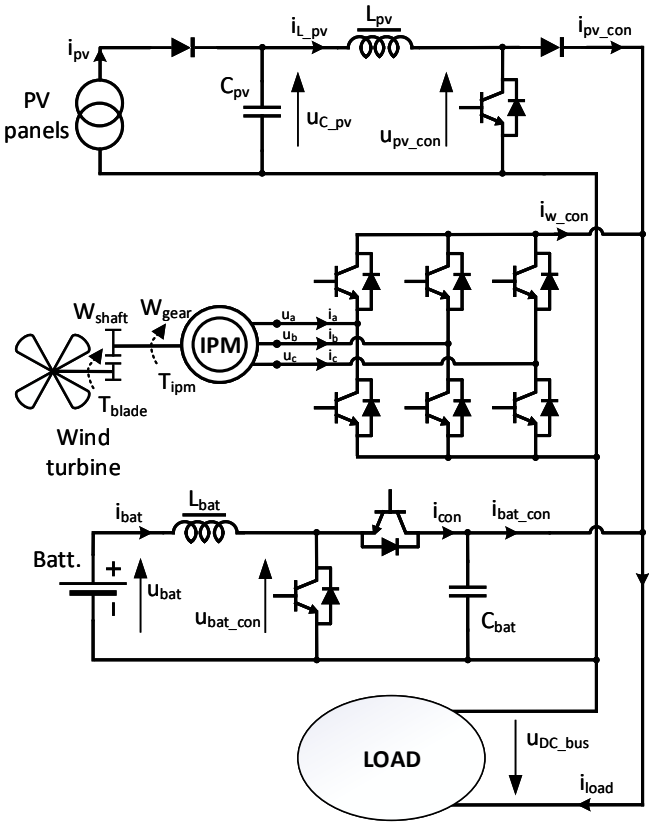

Figure 1: The WSB energy conversion system configuration

organized by EMR and illustrated in Fig. 2. According to the interaction principle, the system can be described as subsystems using four main EMR elements as follows [9]:

- Energy sources with green ovals;
- Accumulation elements are orange rectangles with diagonal line;
- Conversion elements are only orange squares;
- Coupling elements include overlapped orange squares for energy distribution.

All the elements are connected according to the action and reaction principle. The product of action and reaction arrows between two elements results in the instantaneous power exchange. Another key rule of EMR is causality principle, where the output of an accumulation element is an integral function of its inputs.

2.2. Wind Energy Conversion System Modeling

The wind turbine in this study is used to drive an interior permanent magnet (IPM) generator. The wind energy conversion system (WECS) also includes a LC filter to flatten voltage and current, a boost DC/DC converter and diodes to ensure that current flows in only one direction from the source to the DC bus as described in Fig.1. The following model of the WECS was validated in [14, 20]. Hence, this study inherits it to build the WSB system model.

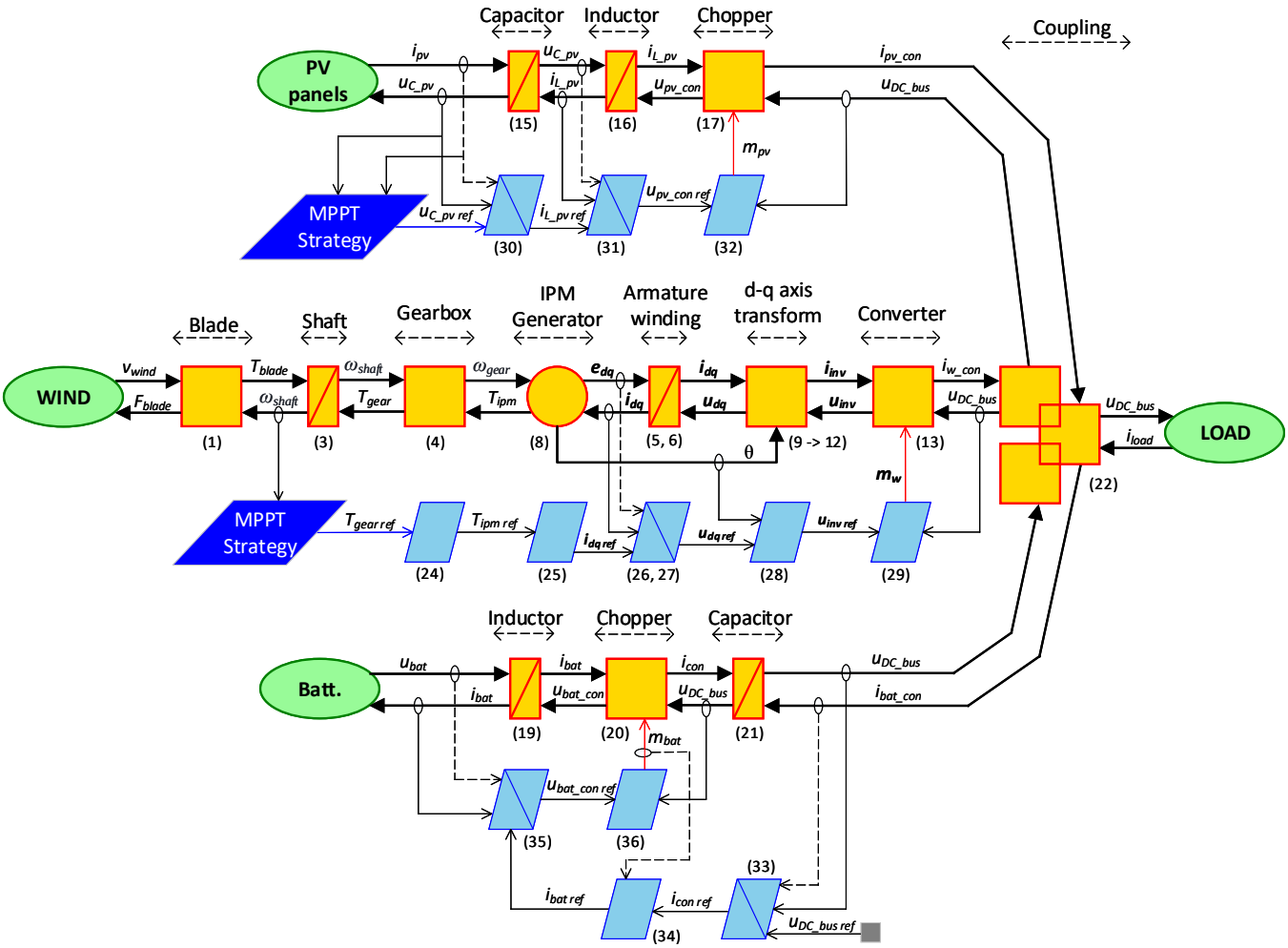

Figure 2: EMR and Inversion-based control of the WSB energy conversion system

2.2.1. Blade

The torque T_{blade} of the blade depends on wind speed v_{wind} and their relationship can be written as below.

$$T_{blade} = \frac{1}{2} C_T \rho S R v_{wind}^2 \tag{1}$$

where C_T is the torque coefficient determined by $C_T - \lambda$ characteristic illustrated in Fig. 3, ρ the air density, R the blade radius, and S the area that the blade sweeps. The the tip-slip ratio λ is defined by the wind and the rotor rotation speed as in (2):

$$\lambda = \frac{R\omega_{shaft}}{v_{wind}}. \tag{2}$$

The force of the blade F_{blade} is also a function of $C_T - \lambda$ which can be defined using Fig. 3.

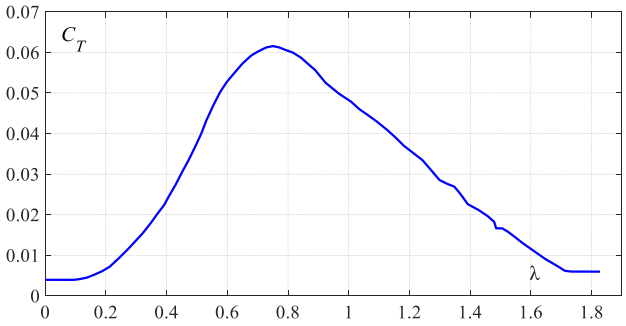

Figure 3: C_T-λ characteristic line [20]

2.2.2. Turbine Shaft and Gearbox

A conventional wind turbine includes a low-speed shaft, a gearbox and a high-speed shaft. The torque balance equation around the low-speed shaft can be written by (3) and represented by an accumulation element.

$$J\frac{d}{dt}\omega_{shaft} = T_{blade} - T_{gear} - f\omega_{shaft}, \tag{3}$$

where J is the moment of inertia of the turbine and f the coefficient of friction. The torque and the angular speed on the shafts of the turbine and the IPM generator are related to the gearbox coefficient k_g as shown below:

$$\begin{cases} \omega_{shaft} k_g = \omega_{gear} \\ T_{ipm} k_g = T_{gear}. \end{cases} \tag{4}$$

2.2.3. IPM generator

The interior permanent magnet (IPM) generator is the element converting rotational movement of the blade caused by the wind into electricity. This type of synchronous machine works frequently along with Maximum power point tracking (MPPT) and maximum torque per ampere (MPTA) methods in wind

energy system because of its significant advantages [19,21,22]. The model of IPM generator includes the stator windings, the rotor flux generation of the permanent magnet and an equation for converting energy from mechanical to electrical [23,24]. The stator winding currents on the rotating d-q axes are calculated according to the equations (5) and (6) below:

$$\begin{cases} i_{sd} = \frac{K}{1+sT_{sd}}(u_{sd} - e_{sd}) \\ i_{sq} = \frac{K}{1+sT_{sq}}(u_{sq} - e_{sq}), \end{cases} \tag{5}$$

$$\begin{cases} K = \frac{1}{R_s};\ T_{sd} = \frac{L_{sd}}{R_s};\ T_{sq} = \frac{L_{sq}}{R_s} \\ e_{sd} = -\omega_s L_{sq} i_{sq} \\ e_{sq} = \omega_s L_{sd} i_{sd} + \omega_s \varphi_p \\ \omega_s = z_p \omega_{gear}. \end{cases} \tag{6}$$

where R_s, L_{sd} and L_{sq} are the resistance and inductance of the armature d-q windings, respectively. With an IPM generator, the rotor flux generation is simply represented with the expression:

$$\varphi_p = \text{cte}. \tag{7}$$

The equation for the transformation of the energy from mechanical to electrical is:

$$T_{ipm} = \frac{3}{2} z_p [\varphi_p i_{sq} + (L_{sd} - L_{sq})\, i_{sd} i_{sq}]. \tag{8}$$

where z_p is the number of pole pairs of the magnet, T_{ipm} the generator torque.

2.2.4. Power Converter

A power converter is used to convert AC electrical power to DC power, which then connect to the DC bus. In the field-oriented control principle, the conversion of the axes from rotating d-q to the three-phase stationary a-b-c is performed the following equations.
The voltage transform is given by:

$$\mathbf{u}_{dq} = \begin{bmatrix} u_{sd} \\ u_{sq} \end{bmatrix} = \mathbf{T}_{P-C} \mathbf{T}_{u_1} \begin{bmatrix} u_{ac} \\ u_{bc} \end{bmatrix}, \tag{9}$$

where

$$\begin{cases} \mathbf{T}_{P-C} = \begin{bmatrix} cos\theta_s & cos(\theta_s - \frac{2\pi}{3}) & cos(\theta_s + \frac{2\pi}{3}) \\ -sin\theta_s & -sin(\theta_s - \frac{2\pi}{3}) & -sin(\theta_s - \frac{2\pi}{3}) \end{bmatrix} \\ \mathbf{T}_{u_1} = \begin{bmatrix} 2 & -1 \\ -1 & 2 \\ -1 & -1 \end{bmatrix}. \end{cases} \tag{10}$$

The current transform is conducted as:

$$\mathbf{i}_{inv} = \begin{bmatrix} i_a \\ i_b \end{bmatrix} = \mathbf{T}_i \mathbf{T}_{C-P} \mathbf{i}_{dq}, \tag{11}$$

where

$$\begin{cases} \mathbf{T}_{C-P} = \begin{bmatrix} cos\theta_s & -sin\theta_s \\ cos(-\theta_s + \frac{2\pi}{3}) & -sin(-\theta_s + \frac{2\pi}{3}) \\ cos(-\theta_s + \frac{4\pi}{3}) & -sin(-\theta_s + \frac{4\pi}{3}) \end{bmatrix} \\ \mathbf{T}_i = \begin{bmatrix} 1 & 0 & 0 \\ 0 & 1 & 0 \end{bmatrix}. \end{cases} \tag{12}$$

Finally, the DC power is archived by the following transform equations:

$$\begin{cases} \mathbf{u}_{inv} = \begin{bmatrix} u_{ac} \\ u_{bc} \end{bmatrix} = \mathbf{m}_w u_{DC\_bus} \\ i_{w\_con} = \mathbf{m}_w^T \begin{bmatrix} i_a \\ i_b \end{bmatrix} \frac{1}{\eta_w^k} = \frac{\mathbf{m}_w^T \mathbf{i}_{inv}}{\eta_w^k} \\ \mathbf{m}_w = \frac{1}{2} \begin{bmatrix} m_{ac} \\ m_{bc} \end{bmatrix}. \end{cases} \tag{13}$$

where $\mathbf{m}_w$ is the modulation function that goes to tuning vector of the converter block and η_w the efficiency of the converter. The coefficient k depends on the power flowing through the converter:

$$k = \begin{cases} 1 & if \quad P > 0 \\ -1 & if \quad P < 0 \end{cases} \tag{14}$$

where P is the power of the converter.

2.3. Solar Energy Conversion System Modeling

The PV panels absorb solar energy and then convert it into electricity. The rest of the system including a LC filter, a boost DC/DC converter and diodes perform similar functions to those of the wind system. The solar energy conversion system (SECS) configuration is indicated in Fig. 1. Similar to the WECS model, this one of SECS is also verified in [20,25] and inherited by this paper.

2.3.1. PV panels

The solar cells system consists of numerous panels connected in series and parallel to provide power to the load. The PV panel in this research is the MSX-83 module of SOLAREX of which characteristics are illustrated in the manufacturer datasheet [26]. It is demonstrated that the current source i_{pv} from PV panels depends on the voltage of panels, environment temperature and the solar radiation.

2.3.2. Capacitor

Similar to C_w, capacitor C_{pv} of solar energy system has the following dynamic model:

$$C_{pv} \frac{d}{dt} u_{C\_pv} = i_{pv} - i_{L\_pv}. \tag{15}$$

2.3.3. Boost converter

The dynamic model of the inductor L_{pv} is obtained by using Kirchhoff's law for the voltage loop.

$$L_{pv} \frac{d}{dt} i_{L\_pv} + R_{L\_pv} i_{L\_pv} = u_{C\_pv} - u_{pv\_con}. \tag{16}$$

The chopper converts the current as well as the voltage at the input of the load by the modulation function m_{pv}. Which is given in below equations:

$$\begin{cases} i_{pv\_con} = \eta_{pv}^k m_{pv} i_{L\_pv} \\ u_{pv\_con} = m_{pv} u_{DC\_bus} \\ 0 \le m_{pv} \le 1 \end{cases} \tag{17}$$

where η_{pv} is the efficiency of the boost converter and the coefficient k depended on the power flowing through the converter is shown in (14).

2.4. Battery System Modeling

2.4.1. Battery

In order to appropriately simplify the system, the battery is considered as a constant voltage source:

$$u_{bat} = \text{cte}. \tag{18}$$

2.4.2. Bidirectional DC/DC Converter

The bidirectional DC/DC converter in this study helps the battery system to both provide power to the load and receive redundant energy from renewable sources. This converter consists of an inductor and two power switches with the topology shown in the Fig. 1. The mathematical model of the inductor L_{bat} is:

$$L_{bat}\frac{d}{dt}i_{bat} + R_{L\_bat}i_{bat} = u_{bat} - u_{bat\_con}. \tag{19}$$

The chopper model is indicated by below equations:

$$\begin{cases} u_{bat\_con} = m_{bat}u_{DC\_bus} \\ i_{con} = \eta_{bat}^{k} m_{ch} i_{bat} \\ 0 \le m_{bat} \le 1 \end{cases} \tag{20}$$

where m_{bat} is the modulation function used to control the switching of power switches of the chopper, η_{bat} the efficiency of this converter and the coefficient k can be determined based on the power flowing through the converter as shown in (14).

2.4.3. Capacitor

The output voltage of the battery system is controlled using a capacitor C_{bat} that has the following dynamic model:

$$C_{bat}\frac{d}{dt}u_{DC\_bus} = i_{bat\_con} - i_{con}. \tag{21}$$

2.5. DC Bus Modeling

The wind system, the solar system and the battery system are connected to a DC bus before supplying power to the load. This parallel connection is modeled by the following equation:

$$i_{load} = i_{pv\_con} + i_{w\_con} + i_{bat\_con}. \tag{22}$$

where i_{load} is the loads current when loads are connected to the DC-link voltage.

3. Control and Management

3.1. Inversion-based Control Design

In this paper, the design of the control structures of the systems is based on the inversion-based control theory. According to this method, the control arrangement of a system is treated as the inversion of the system model in such a way that the control has to determine the suitable inputs calculated from the the subsystem's intended output. There are three rules applied to blue control pictograms of EMR [9]:

- Equations in conversion elements can be inverted directly;
- Feedback controllers are required to invert dynamical subsystems which are represented by accumulation elements;

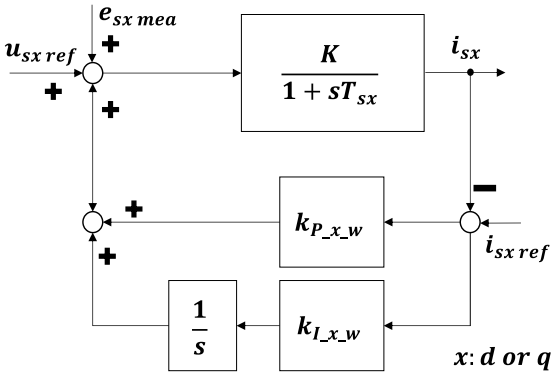

Figure 4: PI current controller for the d-q armature windings

- Inversions of coupling element need the inputs that define the desired energy dispensation.

Each accumulation and conversion orange EMR element is controlled by an control block designed by these above rules. Which are illustrated in Fig. 2. The following system control scheme equations are all listed in Table 1.

3.1.1. Control scheme for wind energy conversion system

Firstly, the desired gearbox torque T_{gear_ref} derived from MPPT strategy block for the wind energy system enters to the direct inversion element of the gearbox to calculate T_{ipm_ref} as in (28). In the scope of this research, it is considered that the generator always works within the rated speed range. Besides, the IPM generator is an conversion element with the Laplace transform dynamic model . Thus, the reference armature current $\mathbf{i}_{dq\_ref}$ is archived by directly inverting the model in (8). Which is based on the first control design rule as shown in equation (29).
The armature d-q windings of IPM generator is an accumulation element with time-dependence model. According to the second inversion control rule, the indirect inversions are performed with proportional-integral (PI) controllers in (30) and (31) to get the desired input $\mathbf{u}_{dq\_ref}$ for the next control element. The PI controller for d-q windings current are synthesized with the structure shown in Fig. 4. The closed transfer function here is:

$$G = \frac{(k_{P\_x\_w} + \frac{k_{I\_x\_w}}{s})(\frac{K}{T_{sx}s+1})}{1 + (k_{P\_x\_w} + \frac{k_{I\_x\_w}}{s})(\frac{K}{T_{sx}s+1})}. \tag{23}$$

Because the control design for d and q armature windings is identical, the symbol x can be replaced by d or q.
Choosing $k_{P\_x\_w}$ and $k_{I\_x\_w}$ so that:

$$\frac{k_{P\_x\_w}}{k_{I\_x\_w}} = T_{sx} \tag{24}$$

then,

$$G = \frac{1}{\frac{1}{Kk_{I\_x\_w}}s + 1} \tag{25}$$

The response time is chosen as $\tau_{res} = \frac{5}{Kk_{I\_x\_w}}$, so the PI con-

Table 1: Equations for systems control scheme

Wind Energy Conversion System	
$T_{ipm\_ref} = \frac{1}{k_g} T_{gear\_ref}$	(28)
$\begin{cases} i_{sd\_ref} = 0 \\ i_{sq\_ref} = \frac{2}{3}\frac{1}{z_p \varphi_p} T_{ipm\_ref} \end{cases}$	(29)
$u_{sd\_ref} = e_{sd\_mea} + k_{P\_d\_w}(i_{sd\_ref} - i_{sd\_mea}) + k_{I\_d\_w}\int_0^t (i_{sd\_ref} - i_{sd\_mea})dt$	(30)
$u_{sq\_ref} = e_{sq\_mea} + k_{P\_q\_w}(i_{sq\_ref} - i_{sq\_mea}) + k_{I\_q\_w}\int_0^t (i_{sq\_ref} - i_{sq\_mea})dt$	(31)
$\mathbf{u}_{inv\_ref} = \mathbf{T}_{u_2}\mathbf{T}_{C-P}\mathbf{u}_{dq\_ref}$	(32)
$\mathbf{m}_w = \frac{\mathbf{u}_{inv\_ref}}{u_{DC\_bus\_mea}}$	(33)
Solar Energy Conversion System	
$i_{L\_pv\_ref} = i_{pv\_mea} - k_{P\_u\_pv}(u_{C\_pv\_ref} - u_{C\_pv\_mea})$	(34)
$u_{pv\_con\_ref} = u_{C\_pv\_mea} - k_{P\_i\_pv}(i_{L\_pv\_ref} - i_{L\_pv\_mea}) - k_{I\_i\_pv}\int_0^t (i_{L\_pv\_ref} - i_{L\_pv\_mea})dt$	(35)
$m_{pv} = \frac{u_{pv\_con\_ref}}{u_{DC\_bus\_mea}}$	(36)
Battery System	
$i_{con\_ref} = i_{bat\_con\_mea} - k_{P\_u\_bat}u_{DC\_bus\_ref} + k_{P\_u\_bat}u_{DC\_bus\_mea}$	(37)
$i_{bat\_ref} = \frac{i_{con\_ref}}{m_{bat}}$	(38)
$u_{bat\_con\_ref} = u_{bat\_mea} - k_{P\_i\_bat}(i_{bat\_ref} - i_{bat\_mea}) - k_{I\_i\_bat}\int_0^t (i_{bat\_ref} - i_{bat\_mea})dt$	(39)
$m_{bat} = \frac{u_{bat\_con\_ref}}{u_{DC\_bus\_mea}}$	(40)

troller coefficients are:

$$\begin{cases} k_{I\_x\_w} = \dfrac{5}{K\tau_{res}} \\ k_{P\_x\_w} = \dfrac{5T_{sx}}{K\tau_{res}}. \end{cases} \tag{26}$$

The other P and PI controllers in this paper can be designed similarly.

The reference 3-phase voltage $\mathbf{u}_{inv\_ref}$ is determined by the direct inversion (32) of axis transformation model with the matrix $\mathbf{T}_{u_2}$ as follows:

$$\mathbf{T}_{u_2} = \begin{bmatrix} 1 & 0 & -1 \\ 0 & 1 & -1 \end{bmatrix}. \tag{27}$$

Lastly, the modulation function of the converter $\mathbf{m}_w$ for WECS is computed by (33) with the measurement of DC-link voltage $u_{DC\_bus\_mea}$.

3.1.2. Control scheme for solar energy conversion system

Firstly, the MPPT strategy block for solar energy system generates the desired voltage of the capacitor $u_{C\_pv\_ref}$ which enters to the indirect inversion element of the capacitor C_{pv}.

After that, the reference inductor current $i_{L\_pv\_ref}$ is get by (34) with the measurements of the capacitor voltage $u_{C\_pv\_mea}$ and the current from PV panels i_{pv_mea}. The P controller here has the gain coefficient $k_{P\_u\_pv}$.

The inductor L_{pv} is also an accumulation element so that the inversion model need a closed-loop control using a PI current controller with the parameters $k_{P\_i\_pv}$ and $k_{I\_i\_pv}$ in (35). The measured current of the inductor and the measured voltage of the capacitor are $i_{L\_pv\_mea}$ and $u_{C\_pv\_mea}$, respectively.

Eventually, the modulation function of the chopper for solar energy system m_{pv} is calculated by (36).

3.1.3. Control scheme for battery system

The DC-link voltage has to be kept stably at a constant value $u_{DC\_bus\_ref}$. The inverted model of the capacitor C_{bat} using a P voltage controller is indicated in (37). The reference current of battery i_{bat_ref} is obtained by the direct inversion model of the chopper as shown in (38).

Then i_{bat_ref} is a input of the indirect conversion element of the inductor L_{bat} along with the measurement of voltage and current of the battery. A PI controller operates to generate the output $u_{bat\_con\_ref}$ from those inputs (39). The bidirectional DC/DC converter of the battery system has the modulation function m_{bat} that is figured out by (40).

3.2. MPPT control strategy

3.2.1. MPPT strategy for wind energy conversion system

Wind energy has a big disadvantage that the wind speed varies, so the power received from the generator is also oscillated. Moreover, wind energy is nonlinear so that it is difficult to establish a linear method for power control. On the other hand, the generated power of the generator depends on the rotor's rotation speed and the wind speed. Therefore, the problem is to find a control algorithm capable of detecting the operating point with maximum power regardless of which generator is used. Thus, MPPT is the suitable solution.

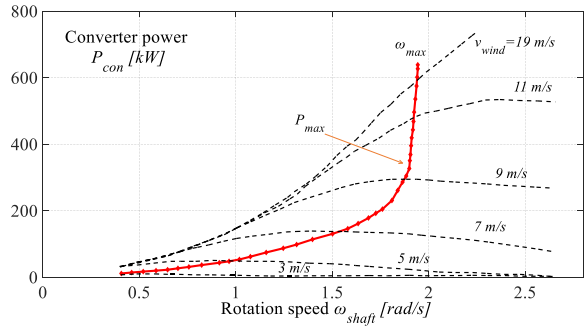

Figure 5: MPPT characteristics of the wind energy system [20]

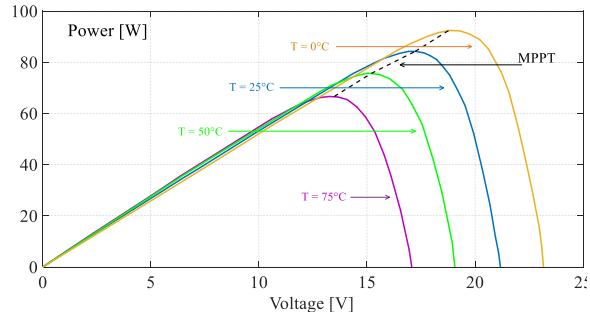

(a) Characteristic P=f(V) of a panel MSX-83 in function of the temperature for a solar irradiance of $1kW/m^2$ [25]

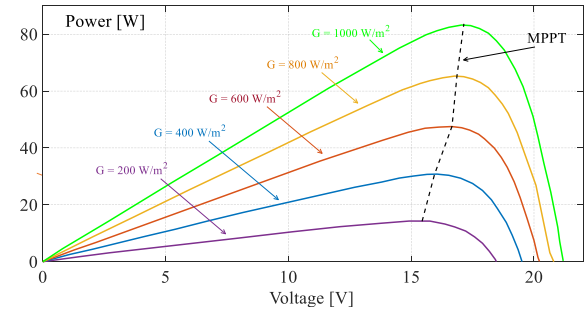

(b) Characteristic P=f(V) of a panel MSX-83 in function of the solar irradiance for a panel temperature of 25 °C [25]

Figure 6: MPPT characteristics of the solar energy system

Based on the specifications of a wind turbine, the power for each wind velocity and rotation speed is able to be figured out in graph form (Fig. 5). The maximum power, which can be extracted for each wind velocity values, is collected. With this characteristic plot, a lookup table is built to express the torque T_{gear_ref} from the measured rotation speed of the turbine rotor ω_{shaft}. Because the MPPT algorithm is not in the scope of this work, the lookup table is used to simplify the simulation. From this method, the designed controllers automatically control the generator output current and voltage so that the received output power corresponding to the wind speed at that time is maximized.

Since the output voltage of the generator change frequently with the wind velocity, it is required to use a chopper along with MPPT strategy not only to obtain maximum power but also to create suitable voltage which is always equal to the DC bus voltage for battery charging.

3.2.2. MPPT strategy for solar energy conversion system

The power from solar panels is also unstable due to the dependence on ambient temperature and solar radiation as mentioned in Section 2. The objective here is to extract the maximum power of the photo-voltaic panels every moment. Hence, the proper solution is also MPPT strategy.
Thanks to the electrical characteristic diagrams of a panel MSX-83, the MPPT characteristics $P = f(V)$ of a photo-voltaic panel are plotted in Fig. 6. From this data, the voltage u_{C_pv} values matching with each maximum power point (MPP) under different environmental conditions are determined by the conventional Perturb and Observe algorithm (P&O) [17]. This tracking work is done by repeatedly increasing or decreasing the output voltage and observing the effect of these disturbance on the power measurement. When the panels power reaches the highest power point, the system operating point will vary near this value.
The boost converter similar to that of the wind energy system is used to support getting the greatest power in each conditions as well as to charge the battery when necessary.

4. Simulation Results

4.1. Evaluation Scenario

The performance of the control system is evaluated by simulation in Matlab/Simulink in the following scenario. At the initial start-up stage, the DC-link voltage increases from 300 V to the set value of 400 V Fig. 10(a). Loads start requesting power from 2.5 seconds Fig. 9(a). Because it is not windy at this time nor radiation from the sun, the battery system is the main energy source for demand of the loads. The wind begins blowing at $t = 5$ s and the PV panels are irradiated from $t = 7$ s. From this moment, solar system and wind system start providing electricity.
The simulation takes place in the changing conditions of natural environmental characteristics affecting the energy conversion system such as wind speed, temperature, solar radiation for a 100-second cycle which are shown in Fig. 7 and Fig. 8.

4.2. Results

With the given simulation scenarios, the required power of isolated loads and the power response of the energy sources are shown in the Fig. 9. During the entire process, the WSB system is always controlled to get the maximum power and provide enough energy for the load with the input from MPPT strategy blocks. The battery system has done a good job of supporting the renewable energy systems, for example between $t = 2.5$ s and $t = 7$ s in the absence of wind and sun or from $t = 30$ s to $t = 45$ s when the energy from sustainable sources is significantly lacking. If the power from wind and solar systems does not meet the consumption demand, the battery system is controlled automatically to supply the loads. In addition, the battery also plays the role of storing energy that the renewable sources produce as function of the weather in the period from $t = 7$ s to $t = 22$ s or at the end of the simulation cycle. That is resulted from the operation of the bidirectional DC-DC converter.
According to the system stability requirements, the DC-link voltage have to be kept in a constant value regardless of the

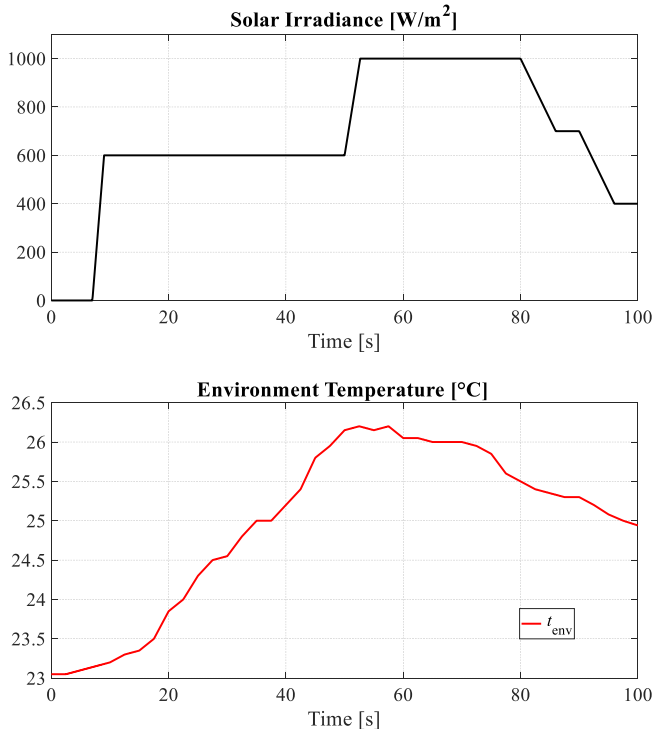

Figure 7: Environment conditions affecting PV panels

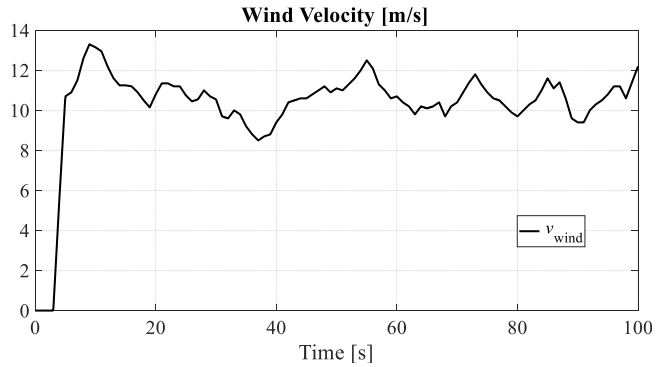

Figure 8: Medium wind velocity characteristics [20]

changing of battery voltage. The simulation results of the DC bus are illustrated in Fig. 10. The DC-link voltage increases to the reference value of 400 V in 0.05 s without overshoot. This voltage response time is the same as τ_{res_vol} which is chosen for the P voltage controller. Even though the loads and the natural conditions affecting solar energy system and wind energy system changes continuously especially from $t = 5$ s to $t = 10$ s as depicted on Fig. 10(b), the voltage controller always operates to stabilize the DC-link voltage at the desired value effectively, i.e. at 400 V.

In order to get the maximum power output, the gearbox torque and PV capacitor voltage must be controlled to follow the computed set value from the MPPT strategy block. The response of T_{gear} and u_{C_pv} are shown in Fig. 11 and Fig. 12, respectively. It can be seen in the Fig. 11 that the gearbox of wind turbine generates the appropriate torque T_{gear} following the desire torque from MPPT strategy block closely. Similarly, the response quality of PV capacitor voltage u_{C_pv} is also a good performance in Fig. 10(b) thanks to the P voltage controller designed for the PV capacitor. The voltage responses to its

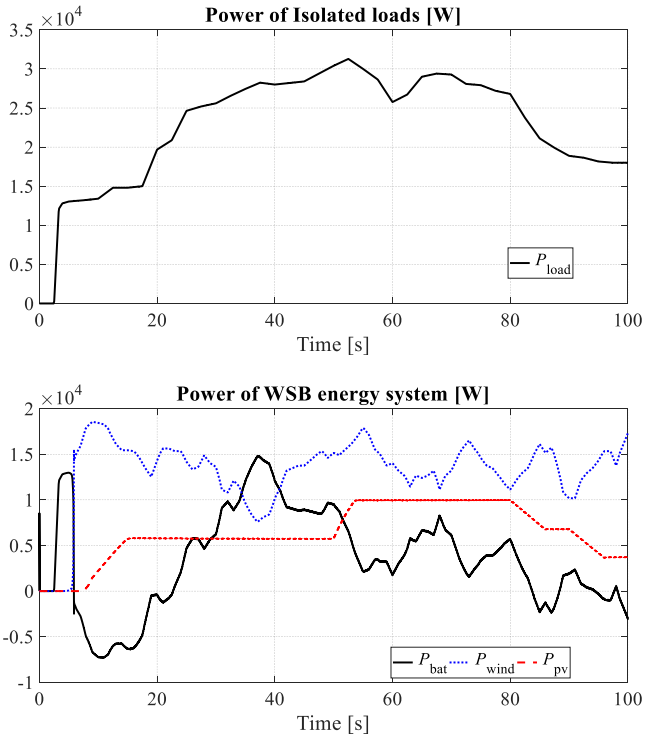

Figure 9: Simulation results of the power supplies system

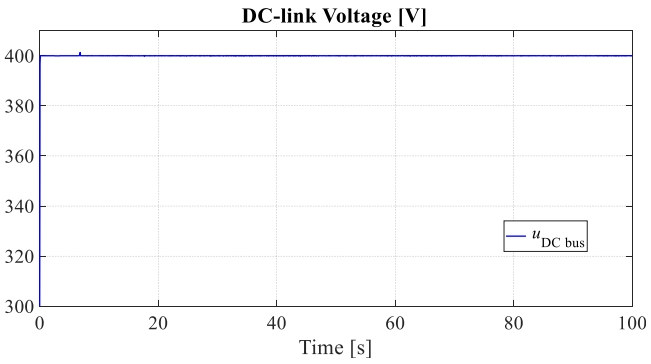

(a) Response to DC-link voltage

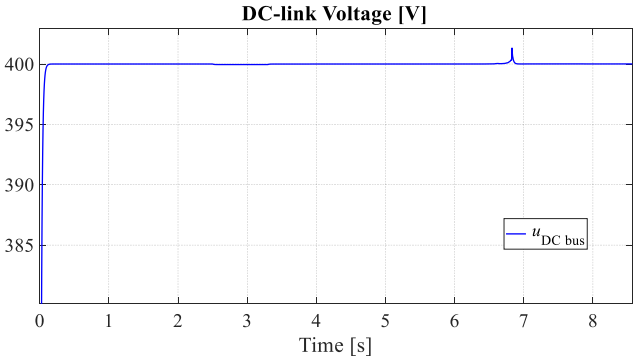

(b) Zoom shape of the response to DC-link voltage

Figure 10: Simulation results of the DC Bus

reference in 0.05 s. All the figures show that the inversion-based controllers make the WSB system operate as planned. Furthermore, these simulation results with EMR lays the basis for feasible implementing the developed control system on a microcontroller or passing it to industrial applications.

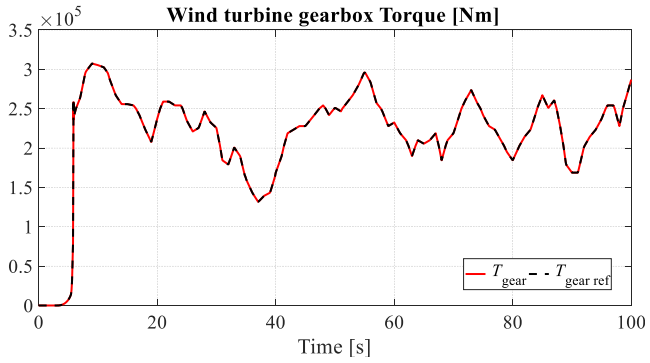

Figure 11: Response to gearbox torque

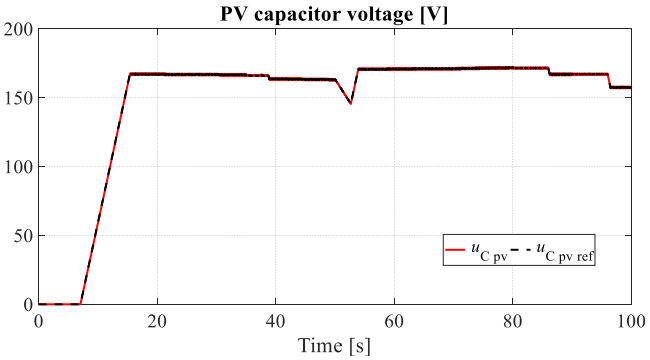

Figure 12: Response to PV capacitor voltage

5. Conclusions

Sustainable energy has been an attractive topic for many years. However, there are still just limited simple but highly effective modeling and control approaches. This paper has taken the advantages of EMR to give an easier but valuable approach to organize a combined renewable energy system. Following that, the system control structure designed by inversion-based control principle shows its reliability and effectiveness when operating in the simulation scenarios based on real conditions. During the simulation, the voltage of the DC bus has always been kept at the reference value by the voltage controller of the battery system, which brings stability to the power supply system. Moreover, conventional MPPT strategies are applied in this study to support the solar energy conversion system and the wind energy conversion system to make the best use of natural energy from wind and solar. In short, all results have demonstrated the positive aspects of the proposed solution.

Acknowledgement

Hoai-Linh T. Nguyen was funded by Vingroup Joint Stock Company and supported by the Domestic Master/ PhD Scholarship Programme of Vingroup Innovation Foundation (VINIF), Vingroup Big Data Institute (VINBIGDATA), code VINIF.2020.ThS.47. This research was supported in part by FCT-Portuguese Foundation for Science and Technology project UIDB/00308/2020, and by the European Regional Development Fund through the COMPETE 2020 Program within project MAnAGER (POCI-01-0145-FEDER-028040).

References

[1] O. Ellabban, H. Abu-Rub, and F. Blaabjerg, "Renewable energy resources: Current status, future prospects and their enabling technology," *Renewable and Sustainable Energy Reviews*, vol. 39, pp. 748 – 764, 2014.

[2] A. Pathak, M. Sharma, and M. Bundele, "A critical review of voltage and reactive power management of wind farms," *Renewable and Sustainable Energy Reviews*, vol. 51, pp. 460 – 471, 2015.

[3] B. Singh, V. Mukherjee, and P. Tiwari, "A survey on impact assessment of dg and facts controllers in power systems," *Renewable and Sustainable Energy Reviews*, vol. 42, pp. 846 – 882, 2015.

[4] R. B. Schainker, "Executive overview: energy storage options for a sustainable energy future," in *IEEE Power Engineering Society General Meeting, 2004.*, vol. 2, 2004, pp. 2309–2314.

[5] S. Chandra, D. F. Gayme, and A. Chakrabortty, "Coordinating Wind Farms and Battery Management Systems for Inter-Area Oscillation Damping: A Frequency-Domain Approach," *IEEE Transactions on Power Systems*, vol. 29, no. 3, pp. 1454–1462, 2014.

[6] B. Li, X. Mo, and B. Chen, "Direct Control Strategy of Real-Time Tracking Power Generation Plan for Wind Power and Battery Energy Storage Combined System," *IEEE Access*, vol. 7, pp. 147 169–147 178, 2019.

[7] N. T. Mbungu, R. Naidoo, R. C. Bansal, and M. Bipath, "Optimisation of grid connected hybrid photovoltaic–wind–battery system using model predictive control design," *IET Renewable Power Generation*, vol. 11, no. 14, pp. 1760–1768, dec 2017.

[8] A. H. Shahirinia, A. Hajizadeh, D. C. Yu, and A. Feliachi, "Control of a hybrid wind turbine/battery energy storage power generation system considering statistical wind characteristics," *Journal of Renewable and Sustainable Energy*, vol. 4, no. 5, p. 053105, sep 2012.

[9] A. Bouscayrol, "Graphic Formalisms for the Control of Multi-Physical Energetic Systems: COG and EMR," in *Systemic Design Methodologies for Electrical Energy Systems*. Wiley, jan 2013, pp. 89–124.

[10] C. Mayet, P. Delarue, A. Bouscayrol, and E. Chattot, "Hardware-In-the-Loop Simulation of Traction Power Supply for Power Flows Analysis of Multitrain Subway Lines," *IEEE Transactions on Vehicular Technology*, vol. 66, no. 7, pp. 5564–5571, 2017.

[11] B. H. Nguyen, R. German, J. P. Trovão, and A. Bouscayrol, "Real-time energy management of battery/supercapacitor electric vehicles based on an adaptation of pontryagin's minimum principle," *IEEE Transactions on Vehicular Technology*, vol. 68, no. 1, pp. 203–212, 2019.

[12] W. Lhomme and J. P. Trovão, "Zero-emission casting-off and docking maneuvers for series hybrid excursion ships," *Energy Conversion and Management*, vol. 184, pp. 427–435, 2019.

[13] J. Solano, D. Jimenez, and A. Ilinca, "A Modular Simulation Testbed for Energy Management in AC/DC Microgrids," *Energies*, vol. 13, no. 16, 2020.

[14] A. Bouscayrol, P. Delarue, X. Guillaud, W. Lhomme, and B. Lemaire-Semail, "Simulation of a Wind Energy Conversion System using Energetic Macroscopic Representation," in *2012 15th International Power Electronics and Motion Control Conference (EPE/PEMC)*, 2012, pp. DS3e.8–1–DS3e.8–6.

[15] T. Yuan, X. Dong, X. Chen, W. Cao, J. Hu, and C. Liu, "Energetic macroscopic representation control method for a hybrid-source energy system including wind, hydrogen, and fuel cell," *Journal of Renewable and Sustainable Energy*, vol. 10, no. 4, p. 43308, jul 2018.

[16] L. Ye, H. B. Sun, X. R. Song, and L. C. Li, "Dynamic modeling of a hybrid wind/solar/hydro microgrid in EMTP/ATP," *Renewable Energy*, vol. 39, no. 1, pp. 96–106, 2012.

[17] M. Zargar, M.-U. D. Mufti, and S. Lone, "Modelling and control of wind solar hybrid system using energy storage system," in *2016 International Conference on Computing, Communication and Automation (ICCCA)*, apr 2016, pp. 965–970.

[18] A. Jahangir and S. Mishra, "Autonomous Battery Storage Energy System Control of PV-Wind Based DC Microgrid," in *2018 2nd International Conference on Power, Energy and Environment: Towards Smart Technology (ICEPE)*, 2018, pp. 1–6.

[19] W. Qiao, L. Qu, and R. G. Harley, "Control of IPM Synchronous Generator for Maximum Wind Power Generation Considering Magnetic Saturation," in *2007 IEEE Industry Applications Annual Meeting*, 2007, pp. 1265–1272.

[20] A. Bouscayrol, X. Guillaud, P. Delarue, and B. Lemaire-Semail, "Energetic Macroscopic Representation and Inversion-Based Control Illustrated on a Wind-Energy-Conversion System Using Hardware-in-the-Loop Simulation," *IEEE Transactions on Industrial Electronics*, vol. 56, no. 12, pp. 4826–4835, 2009.

[21] M. M. Chowdhury, M. E. Haque, M. A. Mahmud, A. M. T. Oo, and A. Gargoom, "Control of IPM synchronous generator based direct drive wind turbine with MTPA trajectory and maximum power extraction," in *2016 IEEE Power and Energy Society General Meeting (PESGM)*, 2016, pp. 1–5.

[22] M. M. Chowdhury, M. E. Haque, S. Saha, M. A. Mahmud, A. Gargoom, and A. M. T. Oo, "An Enhanced Control Scheme for an IPM Synchronous Generator Based Wind Turbine With MTPA Trajectory and Maximum Power Extraction," *IEEE Transactions on Energy Conversion*, vol. 33, no. 2, pp. 556–566, 2018.

[23] Nguyen Phung Quang and D. Jörg-Andreas, *Vector Control of Three-Phase AC Machines*, 2nd ed. Springer-Verlag Berlin Heidelberg, 2015.
[24] R. Krishnan, *Electric Motor Drives: Modeling, Analysis, and Control*, feb 2001.
[25] W. Lhomme, P. Delarue, G. Frédéric, B. Lemaire-Semail, and A. Bouscayrol, "Simulation of a Photovoltaic Conversion System using Energetic Macroscopic Representation," in *15th International Power Electronics and Motion Control Conference and Exposition, EPE-PEMC 2012 ECCE Europe*, sep 2012, pp. DS3e.7–1.
[26] "MSX-83 and MSX-77 Photovoltaic Module," 2015. [Online]. Available: https://www.yumpu.com/en/document/view/37279586/msx-83-and-msx-77-photovoltaic-module-troquedeenergiacom